Surv Geophys (2017) 38:1355–1369
https://doi.org/10.1007/s10712-017-9427-1

Importance Profiles for Water Vapor

Brian Mapes[1] · Arunchandra S. Chandra[1] · Zhiming Kuang[2] · Paquita Zuidema[1]

Received: 20 March 2017 / Accepted: 13 September 2017 / Published online: 7 October 2017

Abstract Motivated by the scientific desire to align observations with quantities of physical interest, we survey how scalar importance functions depend on vertically resolved water vapor. Definitions of importance begin from familiar examples of water mass I^{m} and TOA clear-sky outgoing longwave flux I^{OLR}, in order to establish notation and illustrate graphically how the sensitivity profile or "kernel" depends on whether specific humidity S, relative humidity R, or $\ln(R)$ are used as measures of vapor. Then, new results on the sensitivity of convective activity I^{con} to vapor (with implied knock-on effects such as weather prediction skill) are presented. In radiative-convective equilibrium, organized (line-like) convection is much more sensitive to moisture than scattered isotropic convection, but it exists in a drier mean state. The lesson for natural convection may be that organized convection is less susceptible to dryness and can survive and propagate into regions unfavorable for disorganized convection. This counterintuitive interpretive conclusion, with respect to the narrow numerical result behind it, highlights the importance of clarity about *what is held constant at what values* in sensitivity or susceptibility kernels. Finally, the sensitivities of observable radiance signals I^{sig} for passive remote sensing are considered. While the accuracy of R in the lower free troposphere is crucial for the physical importance scalars, this layer is unfortunately the most difficult to isolate with passive remote sensing: In high emissivity channels, water vapor signals come from too high in the atmosphere (for satellites) or too low (for surface radiometers), while low emissivity channels have poor altitude discrimination and (in the case of satellites) are contaminated by surface emissions. For these reasons, active ranging (LiDAR) is the preferred observing strategy.

✉ Brian Mapes
bmapes@miami.edu

[1] Rosenstiel School of Marine and Atmospheric Sciences, University of Miami, 4600, Rickenbacker Causeway, Miami, FL 33149, USA

[2] Department of Earth and Planetary Sciences, School of Engineering and Applied Sciences, Harvard University, 20 Oxford St., Cambridge, MA 02138, USA

Keywords Water vapor · Humidity · OLR · Convection · Organized convection · Sensitivity · Susceptibility · Functional derivative

1 Introduction

Water vapor in the atmosphere is important for several reasons reviewed well in Sherwood et al. (2010). It carries latent heat that is released upon phase changes. Also, both vapor and condensed water interact strongly with radiation, with at least three major classes of consequences:

a. Direct contributions to global top-of-atmosphere (TOA) radiative energy budgets;
b. Dynamical effects, via both radiative and latent energy budgets in air layers;
c. Observational implications for remote sensing.

Interactions among these effects offer many motivations to deepen our understanding, and many possibilities for research. For instance, mid-level vapor affects low cloudiness, with its strong impacts on global shortwave TOA radiation budgets (Adebiyi et al. 2015; Stevens et al. 2017). Global atmospheric cooling importantly governs precipitation and the hydrologic cycle (e.g., Stephens and Ellis 2008; Previdi 2010; DeAngelis et al. 2015). Convective clouds depend on the vapor field, which in turn is shaped by convective fluxes as well as by latent heating-induced winds that shape transport and surface flux patterns. These couplings make water an intimate active tracer in the atmosphere.

One especially fruitful nexus of interests that can motivate remote sensing is the scientific desire to align observations with quantities of physical interest—or, to turn that around, to cast physical theory in terms of quantities that can be well estimated or strongly constrained from observables. For this reason, item (c) above is kept in context of water's other physical science importances, and is not viewed as a standalone motivation toward measurement for measurement's sake.

2 Simplest: The Profile of I^{m} = Mass Errors from Vapor Measurement Errors

To pursue these ideas quantitatively, it helps to define *importance* (something one cares about) in mathematical terms as a scalar–valued function I with complicated inputs. Such a dimension-reducing function is called a *functional*, and its sensitivities are called *functional derivatives* (see http://www.physicspages.com/2014/11/08/functionals-and-functional-derivatives/). Here we develop notation for how I is distributed over altitude in the atmosphere. From such a framework, progress toward the Grand Challenges motivating this volume can hopefully be steered and assessed.

This paper shows profiles (vertical distributions) of 4 different importances of water vapor at low latitudes. First, I^{m} = column-integrated vapor mass is used to clarify notation and fix ideas. As a second familiar example, I^{OLR} = Outgoing Longwave Radiation (OLR) illustrates the "kernel" approach of Soden et al. (2008). New results are then presented for I^{con} = rainfall (latent heating) by deep convective cloud systems. Finally, I^{sig} = radiative signal in low and high emissivity channels is discussed in the context of observing system design.

For each of these definitions of importance I, we want to know the impact of an increment (or a measurement error) of vapor, as a function of altitude. Such an increment might be expressed as mass (specific humidity S), or relative humidity R, or of some function thereof (for example, increments $\delta\ln(R)$ are relevant to some radiative quantities). In any partial derivative, it is necessary to specify what is held constant, so we will make that part of the mathematical notation where needed for clarity.

In this elementary case, we define an importance scalar or *functional* as I^{m} = column-integrated water vapor mass (CWV, units: kg m^{-2}, or mm of liquid equivalent), sometimes called precipitable water (PW):

$$I^m = \int_0^{p_s} \frac{\mathrm{d}p}{g} \tag{1}$$

where the profile of specific humidity S may be expanded as

$$S(p) = R(p) \times S_{\mathrm{sat}}(T(p), p) \tag{2}$$

Here we ignore any distinction between total pressure p versus the (p) notation for hydrostatic pressure, our monotonic mass coordinate of the vertical domain.

For tropical applications, consider a reference $T(p)$ that is a pseudo-adiabat characterized by its equivalent potential temperature $\theta_{\mathrm{e}} = 350$ K. The corresponding S_{sat} profile is shown in Fig. 1a. The curve to a good approximation decreases linearly with p from 18 g/kg at 1000 hPa to near zero at about 300 hPa.

If a vapor concentration or specific humidity measurement had an error δS, which is constant in height, (1) shows that this error δS would contribute equally from all pressure levels to the error in I^{m}. We denote the accompanying kernel, the sensitivity of vapor mass m to an increment of S, as a functional derivative:

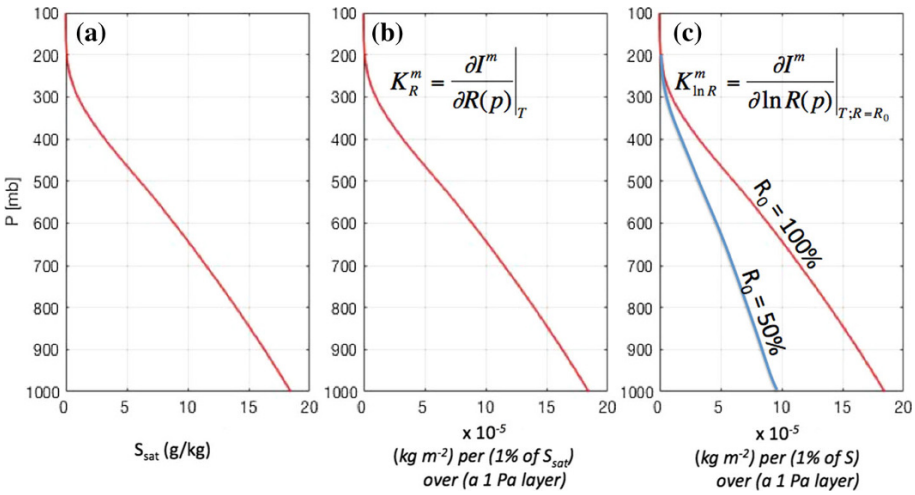

Fig. 1 **a** A reference profile of specific humidity relevant to the tropics: a saturated moist adiabat characterized by $\theta_{\mathrm{e}} = 350$ K. **b**, **c** Kernels expressing the vertical distribution of error in importance function I^{m} = column vapor mass, incurred by measurements with a constant profile of measurement error δR (**b**) or $\delta\ln R$ (**c**)

$$K_S^m \equiv \frac{\delta I^m}{\delta S(p)} \tag{3}$$

Continuous function $S(p)$ notation is retained, even though all calculations below are on discrete levels, to spotlight the distinction between the layer depth appearing in the *units* of the estimated K, versus the vertical resolution of particular discrete calculations used in the estimate.

The functional derivative is defined as the sensitivity when $S(p)$ is held constant at all other altitudes. In our case, S also varies with time, latitude, and longitude, but these need not be specified as being held constant since they are orthogonal to the vertical domain (indexed by hydrostatic p in the usual way). The *value* of (3) is constant in pressure. Its units are (units of Importance) (units of denominator)$^{-1}$ (units of p)$^{-1}$ and the value is equal to 1.02 (kg m^{-2} *of vapor mass*) *per* (1 kg/kg *of S*) *over* (*a* 1 hPa *layer*), since an increment $\delta S = 1$ g/kg over a 10^5 Pa atmosphere equates to $10/9.8 = 1.02$ kg m^{-2} of column vapor mass (mm of liquid equivalent).

Now instead suppose we have a measurement with constant in height *relative* humidity error δR, like the relative humidity sensor in a radiosonde. What is the profile of its contribution to the importance error δI^{m}? That kernel can be notated as:

$$K_R^m \equiv \left.\frac{\delta I^m}{\delta R(p)}\right|_{T=\text{pseudoadiabat@350K}} \tag{4}$$

Here the essential quantity held constant in the partial derivative (T) is specified overtly, as is necessary for clarity in any non-orthogonal "phase space" (Nolte 2010) of abstract variables such as thermodynamic quantities. The units are again (units of Importance) (units of denominator)$^{-1}$ (units of p)$^{-1}$, or (kg m^{-2}) *per* (1% *of* S_{sat}) *over* (*a* 1 Pa *layer*).

Since the contribution of an error δR to $S(p)$, given a fixed $T(p)$, is simply proportional to S_{sat} by Eq. (2), the shape of this kernel (Fig. 1b) is identical to the S_{sat} curve in Fig. 1a. To figure out its value, we can utilize the value of (3) quoted above, noting that where $S_{\mathrm{sat}} = 10$ g/kg (about 650 hPa), a 1% error will equal 10^{-4} kg/kg. Any real instrument's error profile $\delta R(p)$ can be multiplied by the kernel and integrated to give its total importance (in this case, mass error).

Finally, consider the importance of a measurement error in *fractional* R, $\delta\ln(R)$, which is constant with altitude. For saturated spectral bands, the radiative impacts of vapor are sometimes approximated as proportional to $\ln(R)$ (Spencer and Braswell 1997, Pierrehumbert et al. 2007). The desired kernel

$$K_{\ln R}^m \equiv \left.\frac{\delta I^m}{\delta \ln R(p)}\right|_{T=\text{pseudoadiabat@350}K;R} \tag{5}$$

will have units of (kg m^{-2}) *per* (1% *of the existing vapor*) *over* (*a* 1 Pa *layer*). Its derivation can be performed using the chain rule as follows:

$$K_{\ln R}^m \equiv \left.\frac{\delta I^m}{\delta \ln R(p)}\right|_{T;R} = \left.\frac{\delta I^m}{\delta S(p)}\frac{\partial S}{\partial \ln R}\right|_{T;R=R_0} = \left.\frac{\delta I^m}{\delta S(p)} R_0 \frac{\partial S}{\partial R}\right|_T = R_0 K_R^m \tag{6}$$

A new point of notation has been introduced here: the semicolon in the subscript. Items to the right of the semicolon are not *held constant* in the differentiation, they are *evaluated at a given value of* $R(p)$, in this case $R_0(p)$. In this derivation, the core (definitional) dependence of I^{m} on S from (3) is converted into the desired dependence on $\ln(R)$ through a chain rule (first equality). Then, using a calculus fact (second equality), the R dependence

is exposed as a multiplication by $R_0(p)$. At that point, the subscript ;R can be dropped from the last partial derivative.

The final equality simply notes that this result (Fig. 1c) is related to an earlier result (kernel (4), Fig. 1b). Again, we can leverage the values and units above to build this kernel for Fig. 1c.

With these bookkeeping notations and mathematical tools, we can express subtler sensitivities of physical scalars to vapor profiles as functional derivatives.

3 Radiative Kernels: Sensitivity of OLR to Humidity

One familiar climate importance for water vapor is its impact on I^{OLR} = outgoing long-wave radiation (OLR) at top of atmosphere. The dependence of I^{OLR} on the water vapor profile is not a straightforward integral like I^{m}, but rather a result of sophisticated columnar radiative transfer computations. Following Soden et al. (2008), we may characterize this computation's dependencies as $\mathrm{OLR}(T_{\mathrm{em}}(p), S(p), C(p))$, where T_{em} is the emitting temperature of the air, and $C(p)$ is the radiation scheme's own optical measure of cloudiness.

The negative of the zonal and time mean of the TOA OLR kernel for water vapor (Fig. 2 of Soden et al. 2008) is reproduced here as Fig. 2. The negative sign was introduced by Soden et al. (2008) because their application was climate feedback, and *increased* OLR

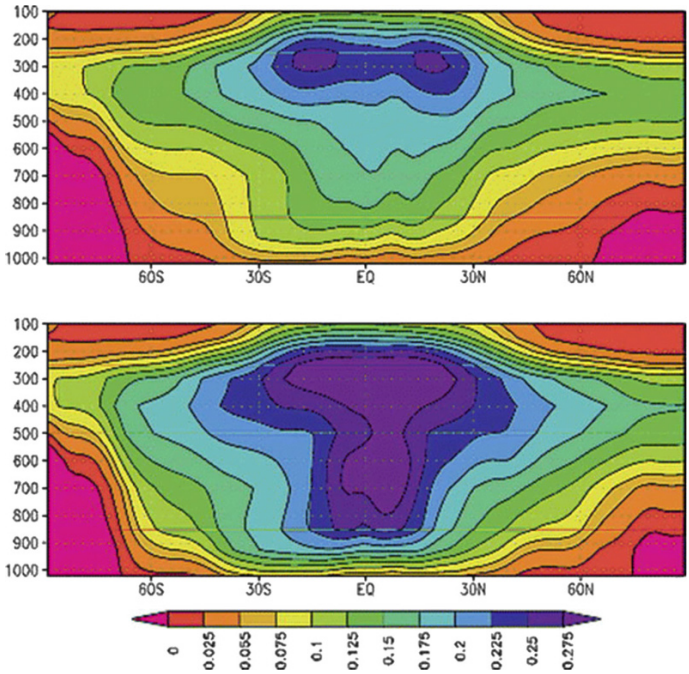

Fig. 2 Soden et al.'s (2008) "kernel" for OLR with respect to water vapor (their Fig. 2), averaged over time and longitude. The top plot is averaged over all-sky conditions (based on a climate model-predicted cloudiness field C) while the lower plot is with cloud radiative effects disabled. Units of the indicated numbers are (W m^{-2}) per (K in the $T_{\mathrm{sat}}(S, p)$ inversion of $S_{\mathrm{sat}}(T, p)$) over (a 100 hPa layer)

is a *negative* contribution to Earth's heat budget. Here we instead use $I^{\mathrm{OLR}} = +\,\mathrm{OLR}$, to express the impact of moisture on the *physical process* of upwelling longwave radiation.

In our notation, the two quantities plotted in Fig. 2 are:

$$K_{T_{\mathrm{sat}}}^{\mathrm{OLR}} = \left.\frac{\delta I^{\mathrm{OLR}}}{\delta T_{\mathrm{sat}}(\phi, p)}\right|_{\{T_{\mathrm{em}}, S, C\} = \mathrm{sim}} \tag{7}$$

and

$$K_{T_{sat}}^{OLR_{clr}} = \left.\frac{\delta I^{OLR}}{\delta T_{sat}(\phi, p)}\right|_{\{T_{em}, S\} = sim, C = 0} \tag{8}$$

where T_{sat} indicates the inversion of the saturation specific humidity function $S(T, p)$ and ϕ is latitude. The set notation $\{\} = \mathrm{sim}$ is used to denote that multiple variables are utilized at climate model-simulated values. For brevity, we have ignored the fact that the kernel computations were done at different longitudes and times, then averaged. The actual computations behind Fig. 2 were performed by probing $\mathrm{OLR}(T_{\mathrm{em}}, S, C)$ with small increments δS at each altitude, with T_{em} and C held constant. Two separate calculations were performed, with C held constant at both realistic model-simulated values ("all-sky") and $C = 0$ ("clear sky" computations). Results of those computations were then recast by those authors, using the chain rule:

$$\left.\frac{\delta I^{\mathrm{OLR}}}{\delta T_{\mathrm{sat}}(\phi, p)}\right|_{T_{\mathrm{em}}, S, C} = \left.\frac{\delta I^{\mathrm{OLR}}}{\delta S(\phi, p)}\right|_{T_{\mathrm{em}}, C; S} \left.\frac{\partial S_{\mathrm{sat}}}{\partial T}\right|_{p} \tag{9}$$

It is important to notice that the *emission* temperature T_{em} was held constant, while T_{sat} was varied for Fig. 2, as the notation emphasizes. Allowing both to vary consistently leads to the well-known cancelation between the *lapse rate feedback* and *water vapor feedback* in climate sensitivity estimation, as discussed in Soden et al. (2008) and elsewhere. Here we wish to characterize I^{OLR}'s dependence on moisture profiles in more direct units of S, R, or $\ln(R)$, holding actual T constant. To do this, we must convert the kernels of Fig. 2 into other units as follows. For definiteness, line plots of the kernel profiles at specific longitudes and months are shown in Fig. 3a (using digital kernel data for two different climate models, downloaded from http://people.oregonstate.edu/~shellk/kernel.html and http://www.rsmas.miami.edu/personal/bsoden/data/kernels.html).

The easiest conversion is simply to reverse the post-processing done by Soden et al., by rearranging Eq. (9) above:

$$K_{S}^{\mathrm{OLR}} = \left.\frac{\delta I^{\mathrm{OLR}}}{\delta S(\phi, p)}\right|_{T_{\mathrm{em}}, C = 0; S} = \left.\frac{\delta I^{\mathrm{OLR}}}{\delta T_{\mathrm{sat}}(\phi, p)}\right|_{T_{\mathrm{em}}, S, C = 0} \left(\left.\frac{\partial S_{\mathrm{sat}}}{\partial T}\right|_{p; T}\right)^{-1} \tag{10}$$

The first factor on the right is kernel (8), the quantity in the bottom panel of Fig. 2 and the top row of Fig. 3. However, the conversion profile (second factor) must be evaluated at some reference profile $T(\phi, p)$, as emphasized with the subscript $;T$. For simplicity, since Fig. shows a tropical point, we use the 350 K pseudo-adiabat again as this reference T profile, a reasonable approximation. We can already anticipate that, since the slope of $S_{\mathrm{sat}}(T)$ increases with T, this factor (the inverse of that slope) will reduce the value of the kernel in the lower troposphere relative to the upper troposphere. In other words: molecule for molecule (or kg for kg), high-altitude vapor is much more important to OLR than low-

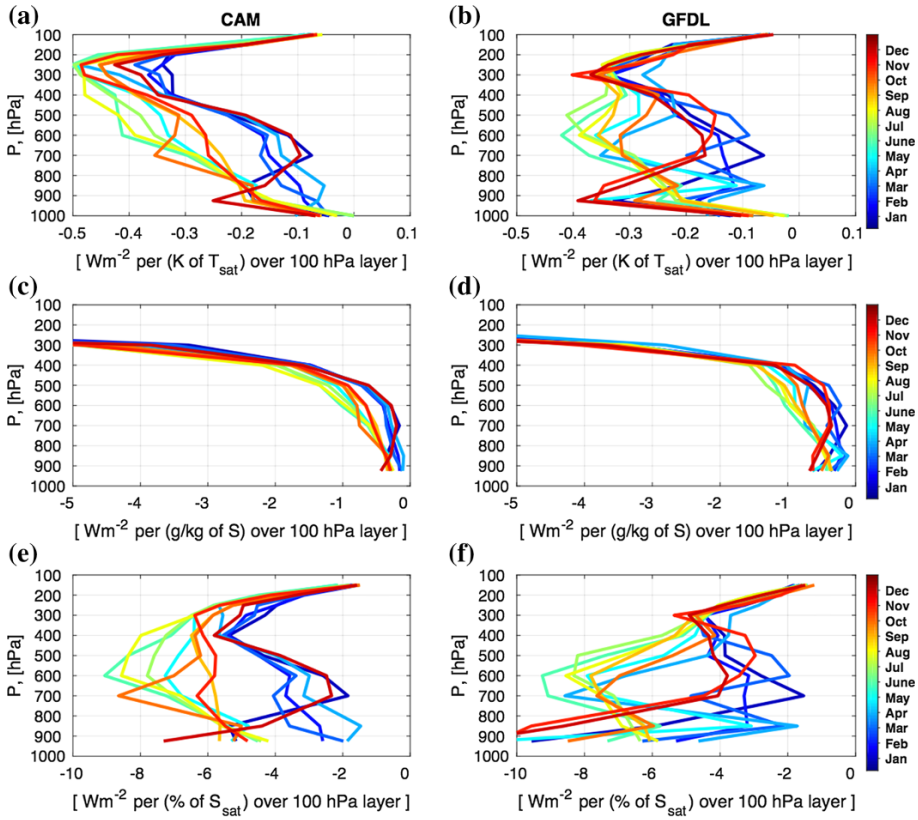

Fig. 3 Top row: The clear-sky kernel of Fig. 2b at a point in the Arabian Sea from **a** CAM and **b** GFDL climate models, using kernel datasets downloaded from the web sites of B. Soden and K. Shell. The twelve colored curves indicate 12 calendar month averages, with dry winter and moist summer monsoon conditions yielding distinctly different sensitivities to increments of moisture. Middle: kernel expressed in terms of increments δS instead using Eq. (10). Bottom: Kernel expressed in terms of increments δR using Eq. (11)

altitude vapor (Fig. 3, middle row), as emphasized in climate literature (e.g., Held and Soden 2000, Allan 2012).

Converting the denominator to reflect the sensitivities of OLR to *relative* humidity increments (δR) is then straightforward, following the steps in Sect. 2:

$$K_R^{\mathrm{OLR_{clr}}} = \left.\frac{\delta I^{\mathrm{OLR}}}{\delta R(p)}\right|_{\{T,S\},C=0} = \left.\frac{\delta I^{\mathrm{OLR}}}{\delta S(p)}\right|_{\{T,S\},C=0} \left(\left.\frac{\partial S}{\partial R}\right|_{T;p}\right) = K_S^{\mathrm{OLR_{clr}}} S_{\mathrm{sat}} \tag{11}$$

Further converting the sensitivity to increments $\delta \ln R$ involves multiplying by a R_0 profile as in (6), which would have to be obtained from these models' climatology of the Arabian Sea:

$$K_{\ln R}^{\mathrm{OLR_{clr}}} = R_0 K_R^{\mathrm{OLR_{clr}}} \tag{12}$$

This final conversion is not shown here, although the seasonality can be imagined in this region with its wet-summer monsoon climate. Even though (as noted above) *molecule for*

molecule, high-altitude vapor is especially important to OLR, the bottom row of Fig. 3 indicates that *an increment of RH in the lower troposphere is approximately as consequential as an increment at other levels* (Held and Shell 2012; Vial et al. 2013). For some measurement systems, the *attribution of altitude to detected water molecules* might be another way to express the important uncertainties incurred in a retrieval process.

4 Importance of Vapor for Deep Convection

Deep convection's sensitivities to water vapor increments (or observation errors) are much less straightforward to estimate than the radiative sensitivities, because "convection" is not an instantaneous, local column process—or even a well-defined one (as elucidated in the Introduction of Sherwood et al. 2010). Simple parcel buoyancy arguments (as embodied in algorithms for convective available potential energy (CAPE) and other simple parcel indices) embody the assertion that only low-level (parcel source level) humidity matters. Indeed, if virtual temperature effects are considered, free-tropospheric moisture *reduces* naïvely computed CAPE. Meanwhile, in reality, mid-level moisture clearly impacts convection positively, as illustrated by the steep dependence of conditional rainfall on column water vapor (Bretherton et al. 2004; Neelin et al. 2009).

The next complexity of a theoretical account is to allow for mixing (entrainment) into updrafts. The buoyancy of a small-scale updraft then depends on humidity in the source layer, as well as in the layers that it has traversed and mixed with. For instance, the steep dependence on column vapor mentioned above may be usefully interpreted as a threshold-like dependence on parcel source-level humidity, plus a linear dependence on humidity in the free troposphere above that (Muller et al. 2009). Microphysical processes such as precipitation shedding during the finite time of parcel ascent are another ambiguity in determining bulk density and thus parcel buoyancy.

Even such a dressed-up (mixing-allowing, microphysics-respecting) parcel theory remains badly incomplete, however. The "importance" of convection as a process lies not in the fate of one hypothetical lone updraft, but rather in the time-integrated, net behavior of *ensembles* of convective *circulations* (perhaps in a scale-truncated sense) that must obey mass continuity in a particular geometrical configuration. Essentially, the kernel we seek is a subset of the cumulus parameterization problem (Arakawa 2004). For this reason, explicit convection-permitting models (CPMs) are needed to fill the gap between parcel theory and reality in estimating our desired sensitivity kernel, or even defining it with sufficient specificity.

In a convecting atmosphere, a humidity increment provokes a complex time-dependent and multi-scale response that includes thermally driven large-scale ascent as well as local cloud-scale overturnings. Observationally, all this is further superposed with noise. Simple regression of local convection measures on humidity observations thus gives us only a faint and distorted glimpse of moisture's true impact on convection (as discussed in Mapes et al. 2017). Active probing of models is required to even begin to interpret observations properly.

Early computation-limited studies used short integrations over small domains, in an *initial-value* approach with newly triggered convection, in 2D (Nicholls et al. 1988) or 3D (Takemi and Satomura 2000). Mapes (2017) discusses in more detail how domain constraints translate into function or importance measures. As computers have advanced, fully developed convection fields in larger and longer runs have been probed, for instance using

humidity field relaxation experiments (Derbyshire et al. 2004 in that special issue) or transient impulses (Tulich and Mapes 2010; Kuang 2010). Long-time integrations make cyclic boundary conditions appealing for conservation reasons. The unreality of cyclicity is compensated by forcing applied through time, which subtly but profoundly reshapes the questions being asked and addressed. Taken together, all these approaches indicate that GCM convection parameterizations almost universally have inadequate sensitivity to mid-level moisture, rooted foreseeably in their use of simplistic updraft instability indices. However, offering a better quantitative estimate is more difficult than offering a critique.

Because deep convection is a "noisy" process, with lots of internal free variability, *ensemble* runs of cyclic CPMs (CCPMs), each with its internal ensemble of convective circulations, are required to find the systematic response. But although the response of convection to humidity is not very *deterministic*, its expectation value is very *linear* (Tulich and Mapes 2010). Unfortunately, probing such an ensemble produces large numbers of time-dependent responses that are difficult to summarize. However, the mathematical linearity of responses opens another avenue.

That linearity was exploited by Kuang (2010) to construct a time-invariant linear response matrix $\mathbf{M}$ through an elegant matrix inversion procedure. The time-dependent responses mapped by Tulich and Mapes (2010) were shown to be merely a facet of $\mathbf{M}$, specifically $\exp(\mathbf{M}t)$, as illustrated in his Appendix. A finite-time propagator matrix $\mathbf{G} = (\exp(\Delta t \cdot \mathbf{M}) - \exp(0 \cdot \mathbf{M}))/\Delta t$ is another facet of $\mathbf{M}$, and such matrices for $\Delta t = 4$ h are depicted in Fig. 8 of Kuang (2012).

Here let us define I^{con} = *rainfall anomalies over the subsequent* 3 h in a convecting patch of atmosphere of size $o(10^2\text{–}10^3)$ km. Our desired kernel or sensitivity profile can be obtained by integrating one quadrant of $\mathbf{G}$ over atmospheric mass. But what has been held constant in such a computation? An important part of the answer is *domain-averaged vertical motion* $[w] = 0$ *at all altitudes*, by the cyclic boundary conditions of a CCPM. All the other parameters specified in running the CCPM are also important, such as domain geometry and size. The kernel we seek can be expressed as:

$$K_S^{\mathrm{con}} = \left.\frac{\delta I^{\mathrm{con}}}{\delta S(p)}\right|_{RCE:\{[w]=0,\mathrm{geometry},\mathrm{SST},Q_{\mathrm{rad}},\ldots\}} \tag{13}$$

where the set of conditions $\{\ldots\}$ for the radiative-convective equilibrium (RCE) reference state includes all of the parameters of the CCPM's forcing and configuration.

To better appreciate the role of domain geometry, consider two RCE configurations: 128 km × 128 km isotropic flow with no wind shear to break symmetry, and 2048 km × 64 km, also unsheared. Column water vapor maps for a 2048 km square sample of these two unbounded (but cyclic) domain symmetries are shown in Fig. 4. Domain-mean profiles are inset. Two differences are obvious: (1) convection is "organized" in the sense of *quasi-two-dimensional* in the long-domain run, and (2) the long-domain average is warmer and drier, because a large area with thermally capped (stable) dry air contributes a lot toward the domain average. One way to look at this is that the ensemble of convective circulations defining I^{con} has all the descending branches concentrated and reinforcing each other in the long domain, rather than distributed randomly and canceling each other as they do in the isotropic domain. This is a symmetry condition as in crystallography, not a domain "size" issue per se, since both atmospheres are really horizontally unbounded.

The kernel (13) differs substantially between these two cases, as seen in the right-hand panels of Fig. 5b, d. The left panels of Fig. 5a, c also show the sensitivity to temperature

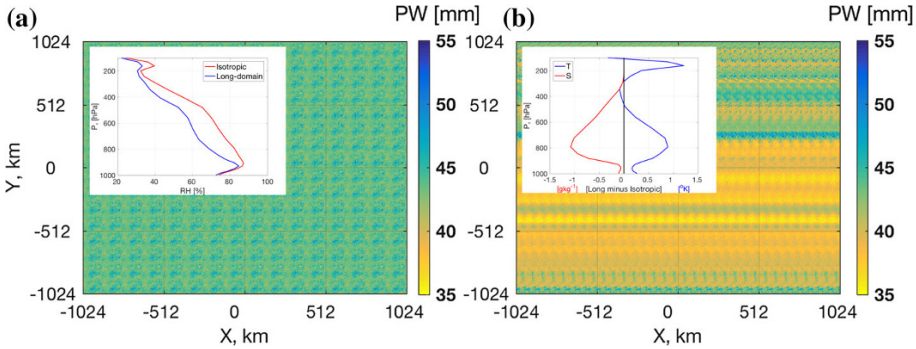

Fig. 4 Column water vapor maps for 2048 × 2048 km samples of the unbounded atmospheres embodied by cyclic cloud-permitting model (CCPM) simulations with **a** 128 × 128 km grid and **b** 2048 × 64 grid. Grid mesh size is 2 km in all cases. Inset line plots show that the domain average of the long domain with "organized" convection is warmer and drier in the lower free troposphere, as well as warmer near the tropopause

for completeness (discussed briefly below, as this is a novel result). The plot titles emphasize Unorganized (isotropic) versus Organized (long) geometries as the nature of the difference, but interpretation must be considered more carefully than that. The units in Fig. 5 should be self-explanatory after the discussions above.

Consider first the Unorganized sensitivity profiles in Fig. 5a, b, derived from the isotropic CCPM of modest size (128 km) with no wind shear. Convection consists of intermittent scattered cumulonimbus (Cb) clouds. As predicted by parcel notions of buoyant moist convection, an increment of water vapor δS in the lowest kilometer or two has the biggest effect, but the same δS of vapor added to other levels still has a positive effect. All levels above about 700 hPa are about equally important to rainfall production (panel 5b), in this geometry and RCE base state. Temperature sensitivity can be similarly understood in parcel buoyancy terms (panel 5a). There is positive sensitivity to temperature in the low-level parcel source layer, while ambient environment warmth from 900 to 500 hPa acts to reduce parcel buoyancy, an "inhibition" effect, but one that is much deeper than naïve undiluted parcel computations would suggest.

By contrast, Organized convection (long domain, panels 5c, d) is much more sensitive to water vapor increments at all levels, especially in the free troposphere (panel 5d). In this elongated domain (sometimes called "bowling-alley" geometry), convective circulations necessarily take the form of squall-like "layer overturning" (Kuang 2012) rather than sporadic buoyant parcel ascent. Interpretation therefore must recognize such layer overturning as the system whose response to a horizontally uniform increment δS is being measured. Such a horizontally uniform perturbation may seem like a fiction, but could perhaps be viewed as being generated by advection by a much larger-scale adiabatic vertical motion.

In the long geometry, a deep *layer* of lower-tropospheric air is rising, so enhanced humidity or temperature in that layer can enhance domain-mean precipitation for reasons that do not involve horizontal mixing (entrainment) into a convective-scale buoyant updraft. Apparently for this reason, humidity and temperature sensitivities are strong and positive up to 700 hPa. Upper-tropospheric δS increments also have a very strong impact on domain precipitation (panel 5d), presumably by enhancing stratiform precipitation from upper-level stratiform cloud (Houze 1997) and not from mixing effects on buoyancy in the upper levels of Cb updrafts. Upper-level temperature has a negative impact. Might that also be interpreted as an effect involving the precipitating upper-level stratiform cloud, or is it

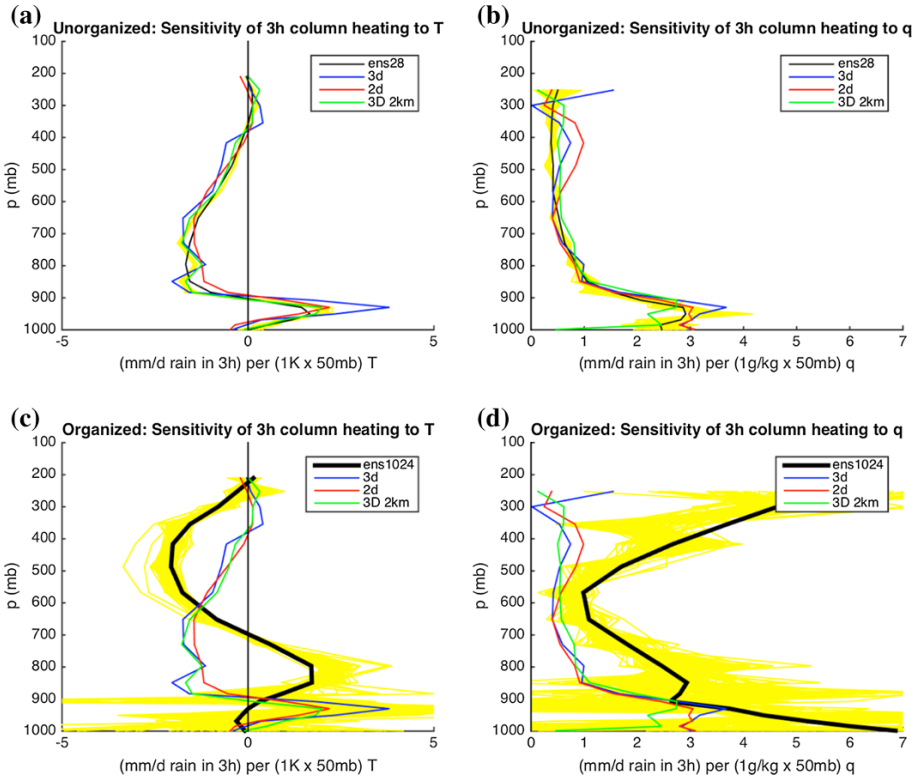

Fig. 5 Profiles of the importance of an increment of temperature (left) or water vapor (right) at any given altitude to rainfall rate (expressed in mm/day) averaged over the subsequent 3 h. Results are for a cyclic convection-permitting model at equilibrium with a forcing that produces a rainrate of about 4 mm/day. Top row: Unorganized refers to convection in small cyclic domains with no wind shear. Black curve and yellow band show estimates from ensembles of simulations. Early estimates made with smaller domains and a 2-dimensional computation (blue, green, red) are repeated in both panels for reference. Bottom row: Organized refers to convection in a 2048 × 64 km elongated cyclic domain. An ensemble approach has been used to estimate uncertainty (yellow) around a lightly vertically smoothed mean estimate (heavy black curve)

again an "inhibition" effect on convection—a reduction of the updraft buoyancy that is the ultimate energy source for the convective circulation (through the buoyancy flux b'w' source term in the kinetic energy equation)?

Our take-away lessons about moisture sensitivity must notice that the domain-mean condition is very much drier in the "Organized" (long domain) case (insets to Fig. 4), or to put it more sharply, *organized convective systems can exist in drier mean conditions than ordinary convection* (Takemi and Satomura 2000). In these CCPMs, background $S(p)$ is not imposed, and cannot easily be changed without breaking the equilibrium condition of RCE, so this is a result in itself. In nature, the asymptotically long-time equilibrium of the moisture field enforced in steady CCPM runs is rarely or never observed on the scales of Fig. 4b. In the burgeoning literature on radiative-convective equilibrium (RCE) (Wing et al. 2017; Mapes 2016), the >20 mm dynamic range of column water vapor (CWV) in Fig. 4 would take many days to develop, making it an artifact of cyclic boundaries that may not directly correspond to nature (Holloway et al. 2017).

If the most important result of these experiments is that organized convection can survive in drier environments, the functional lesson for nature might be that it is *less sensitive to dryness* than ordinary convection—opposite in sense from the face value of Fig. 5 (enhanced sensitivity). For instance, the ability of quasi-2D squalls to survive hostile environments can widen the time-mean tropical rainfall belt relative to its treatment only as vertical plume convection (Nolan et al. 2016). Sahelian Africa may similarly be the beneficiary of rain from organized storms, in environments too dry to support local vertical precipitating convection (e.g., Section 5 of Nicholson 2013).

To re-express the denominator of these kernels in terms of δR would involve multiplying them by $S_{\mathrm{sat}}(T)$, making them much more bottom-heavy, as in the middle to bottom row differences of Fig. 3. This is a useful insight: it actually takes a very large or even unrealizable RH perturbation to account for 1 g/kg of δq in the middle or upper troposphere, as postulated in the units of Fig. 5, so the large kernel values at upper levels in Fig. 5b. may be somewhat irrelevant in practical terms.

5 Importance Functions for Passive Remote Sensing

To extend the radiative reasoning of Sect. 3, consider another Importance function: I^{sig} = signal detected by some instrument. Figure 6 sketches kernel profiles for I^{sig} = -brightness temperature for down-looking microwave instruments in spectral regions where water vapor has low (cyan, purple) and high (blue) emissivity. In this figure (following

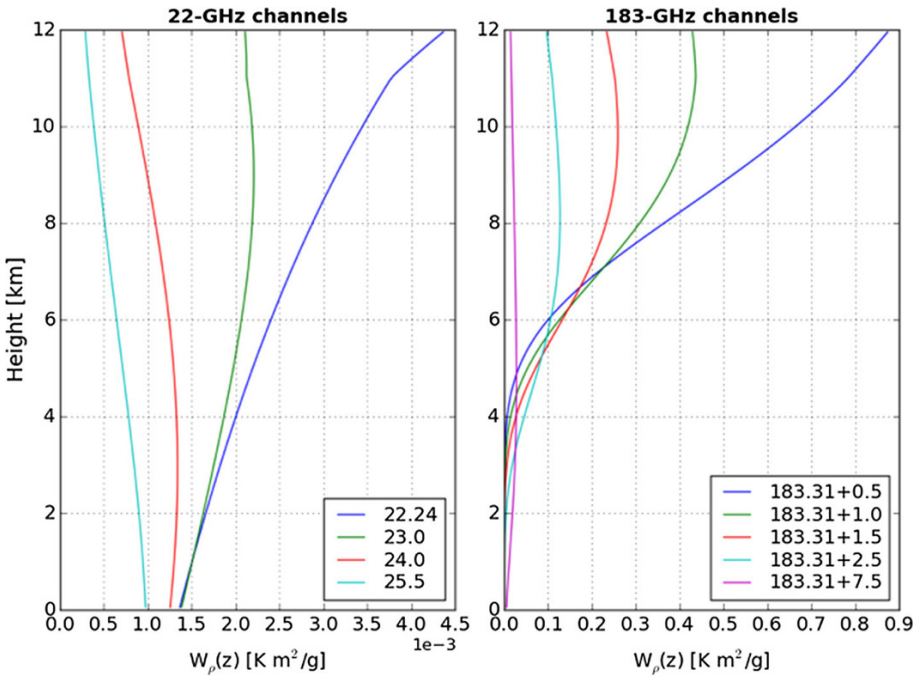

Fig. 6 Contributions of water vapor to brightness temperature seen from above, as a function of altitude, in **a** low and **b** high emissivity channels, with a radiatively cold background (water, with its high reflectivity and thus low emissivity). Conventions as in Mech et al. (2014)

Mech et al. 2014), our "kernel" K is depicted as a "weighting function" W, whose denominator is calibrated to increments not of S or R but of vapor density ρ.

$$K_{\rho}^{\mathrm{sig}} = \left.\frac{\delta I^{\mathrm{sig}}}{\delta \rho_v(z)}\right|_{\{T,\mathrm{backdrop}\};\rho} \equiv W_{\rho}(z) \tag{14}$$

The units can be unpacked as (K of signal) per (1 g m^{-3}) over a (1 m layer), while the small 1e−3 label clarifies that the axis numbers are really over a 1 km layer. Perhaps more clearly, it can be read as (K of signal) per (1 kg m^{-2} of a local *layer* of vapor mass, centered at each altitude).

In the limit of low emissivity in the measurement band, every molecule of vapor sends photons to the detector with equal efficiency, with no blockage by the intervening vapor. The cyan curve is near this limit and is greater at low levels because the emitting temperature is greater there, not because distant molecules are more efficacious than close ones at contributing to the detected signal. Meanwhile, the higher the emissivity in the band being observed, the more the photons come solely from the vapor nearest the detector, as indicated by blue curves for high emissivity bands. Using high emissivity bands, multichannel passive sensors can achieve fine vertical resolution, but only in a robust manner in areas close to the sensor.

Unfortunately, the only way to achieve fine resolution far from a passive sensor is through the error-prone differencing of highly overlapping kernels. In the downward-looking case, surface emission introduces further errors and ambiguities to such an exercise. As a result, no combination of kernels like Fig. 6 will yield good profile resolution and accuracy at low-middle levels, as desired based on the motivating physical process sensitivity kernels above. Upward-looking passive sensors could utilize high emissivity channels to achieve high resolution near the surface, but vertical discrimination in the lower free troposphere is harder, and made harder still by the decrease in both S and the emitting temperature with altitude. In practice, conventional microwave sensors achieve only about 2–3 distinct degrees of freedom in whole-troposphere moisture profiling (Brogniez et al. 2016; Zhang et al. 2017; see also Fig. 1 of Pincus et al. 2017, this volume).

While hyperspectral passive methods with very high sensitivity and precision can improve on existing technology, it seems clear that the best way to probe vertically resolved vapor in the lower free troposphere is with active sensors (Nehrir et al. 2017, see also Fig. 10 of Stevens et al. 2017; both in this volume). Light Detection And Ranging (LiDAR) and its radio cousin (RADAR) systems use time (range) gating to achieve the desired vertical resolution. Limb occultation uses angular geometry (see also Fig. 3 of Pincus et al. 2017, this volume). One challenge of LiDAR is to achieve sensitivity across a wide dynamic range: to best serve our needs, radiation must get through intervening layers, twice, and still interact to an accurately measurable degree with vapor in the desired mid-tropospheric layers. These may be quite dry, and yet the physical importance of accuracy may grow with background dryness, for instance in their radiative importance (Spencer and Braswell 1997; Pierrehumbert et al. 2007), raising the demands on laser power and/or detector sensitivity, especially when looking upward from the surface through optically thick intervening layers. Spaceborne active platforms have an advantage in this regard, and the use of multiple frequencies helps break up the extreme dynamic range challenge into more tractable chunks (Fig. 1 of Nehrir et al. 2017, this volume).

Radiative cooling of clouds at the top of the planetary boundary layer (PBL) is crucial to their dynamics, longevity, vigor, albedo, and thereby to the climate impact they exert in the visible spectrum (rejecting sunlight). Low-middle troposphere vapor is thus especially

important to these clouds, by modulating cloud-top cooling, as discussed in Stevens et al. (2017) and elsewhere. Yet these are precisely the altitudes and dry conditions for which vapor measurement physics poses the greatest bind for both passive and active measurements, as sketched in the paragraphs above. Here lies an especially enticing opportunity for technological glory.

Designing such glorious systems will require a clear view of "importance" functions of vapor for both physical climate system impacts (radiation and convection) and detectability. It is hoped that this paper may help to clarify the challenge and the hopes for surmounting it.

6 Summary and Conclusions

We have explored the sensitivity of important processes (measured by scalars) to water vapor as a function of height. In every case, lower-middle troposphere is important. Unfortunately, passive measurements are poor for this region of the atmosphere. Active sensing (see Nehrir et al. 2017) is advocated as a crucial technology approach to improve measurements and, thereby, our understanding of important processes. Synthesis of all observations within atmospheric analysis systems will be a final challenge, with modeling as well as detection aspects (Pincus et al. 2017, this volume), but is a path to demonstrate such understanding as a powerful estimation and prediction capability in regions beyond the observed.

Acknowledgements This article is based on work supported by U.S. NOAA Grant NA13OAR4310156 and NASA Grant NNX15AD11G. Mario Mech kindly contributed the unpublished Fig. 6, related to a similar figure in Mech et al. (2014). We are grateful for comments by Bjorn Stevens, Robert Pincus, and anonymous reviewers whose efforts greatly improved the manuscript.

References

Adebiyi AA, Zuidema P, Abel SJ (2015) The convolution of dynamics and moisture with the presence of shortwave absorbing aerosols over the southeast Atlantic. J Clim 28:1997–2024. doi:10.1175/JCLI-D-14-00352.1

Allan RP (2012) The role of water vapour in Earth's energy flows. Surv Geophys 33(3–4):557–564

Arakawa A (2004) The cumulus parameterization problem: past, present, and future. J Clim 17:2493–2525

Bretherton CS, Peters ME, Back L (2004) Relationships between water vapor path and precipitation over the tropical oceans. J Clim 17:1517–1528

Brogniez H, Fallourd R, Mallet C, Sivira R, Dufour C (2016) Estimating confidence intervals around relative humidity profiles from satellite observations: application to the SAPHIR sounder. J Atmos Ocean Technol 33:1005–1022. doi:10.1175/JTECH-D-15-0237.1

DeAngelis AM et al (2015) An observational radiative constraint on hydrologic cycle intensification. Nature 528:249–253

Derbyshire S, Beau I, Bechtold P, Grandpeix J-Y, Piriou J-M, Redelsperger J-L, Soares P (2004) Sensitivity of moist convection to environmental humidity. Q J R Meteorol Soc 130:3055–3079. doi:10.1256/qj.03.130

Held IM, Shell KM (2012) Using relative humidity as a state variable in climate feedback analysis. J Clim 25(8):2578–2582

Held IM, Soden BJ (2000) Water vapor feedback and global warming. Annu Rev Energy Environ 25:441–475

Holloway CE, Wing AA, Bony S, Muller C, Masunaga H, L'Ecuyer TS, Turner DD, Zuidema P (2017) Observing convective aggregation. Surv Geophy. doi:10.1007/s10712-017-9419-1

Houze RAJ (1997) Stratiform precipitation in regions of convection: a meteorological paradox? Bull Am Meteorol Soc 78:2179–2196

Kuang Z (2010) Linear response functions of a cumulus ensemble to temperature and moisture perturbations and implications for the dynamics of convectively coupled waves. J Atmos Sci 67:941–962

Kuang Z (2012) Weakly forced mock-Walker cells. J Atmos Sci 69:2759–2786

Mapes BE (2016) Gregarious convection and radiative feedbacks in idealized worlds. J Adv Model Earth Syst. doi:10.1002/2016MS00065

Mapes BE (2017) Toward form-function relationships for mesoscale structure in convection: a review. J Meteorol Soc Jpn (**submitted**)

Mapes BE, Chandra A, Kuang Z, Song S, Zuidema P (2017) Estimating convection's moisture sensitivity: a model-observation synthesis using DYNAMO data. J Atmos Sci (**in preparation**)

Mech M, Orlandi E, Crewell S, Ament F, Hirsch L, Hagen M, Peters G, Stevens B (2014) HAMP the microwave package on the high altitude and long range research aircraft HALO. Atmos Meas Tech 7:4539–4553. doi:10.5194/amt-7-4539-2014

Muller CJ, Back LE, O'Gorman PA, Emanuel KA (2009) A model for the relationship between tropical precipitation and column water vapor. Geophys Res Lett 36:L16804. doi:10.1029/2009GL039667

Neelin JD, Peters O, Hales K (2009) The transition to strong convection. J Atmos Sci 66:2367–2384. doi:10.1175/2009JAS2962.1

Nehrir AR et al (2017) Emerging technologies and synergies for airborne and space-borne measurements of water vapor profiles. Surv Geophy. doi:10.1007/s10712-017-9436-0 **(this volume)**

Nicholls ME, Johnson RH, Cotton WR (1988) The sensitivity of two-dimensional simulations of tropical squall lines to environmental profiles. J Atmos Sci 45:3625–3649. doi:10.1175/1520-0469(1988)045<3625:TSOTDS>2.0.CO;2

Nicholson SE (2013) The West African Sahel: a review of recent studies on the rainfall regime and its interannual variability. ISRN Meteorol, vol. 2013, Article ID 453521. doi:10.1155/2013/453521

Nolan DS, Tulich SN, Blanco JE (2016) ITCZ structure as determined by parameterized versus explicit convection in aquachannel and aquapatch simulations. J Adv Model Earth Syst 8:425–452. doi:10.1002/2015MS000560

Nolte DD (2010) The tangled tale of phase space. Phys Today 63:33–38

Pierrehumbert RT, Brogniez H, Roca R (2007) On the relative humidity of the Earth's atmosphere. In: Schneider T, Sobel A (eds) The global circulation of the atmosphere: phenomena, theory, challenges. Princeton University Press, Princeton

Pincus R et al (2017) The representation of tropospheric water vapor over low-latitude oceans in (re-)analysis. Errors, impacts, and the ability to exploit current and prospective observations. Surv Geophys. doi:10.1007/s10712-017-9437-z **(this volume)**

Previdi M (2010) Radiative feedbacks on global precipitation. Environ Res Lett 5:025211. doi:10.1088/1748-9326/5/2/025211

Sherwood SC, Roca R, Weckwerth TM, Andronova NG (2010) Tropospheric water vapor, convection, and climate. Rev Geophys 48(2):RG2001. doi:10.1029/2009RG000301

Soden B, Shell Karen M, Kiehl Jeffrey T, Shields Christine A (2008) Quantifying climate feedbacks using radiative kernels. J Clim 21:3504–3520. doi:10.1175/2007JCLI2110.1

Spencer RW, Braswell William D (1997) How dry is the tropical free troposphere? Implications for global warming theory. Bull Am Meteorol Soc 78:1097–1106. doi:10.1175/1520-0477

Stephens GL, Ellis TD (2008) Controls of global-mean precipitation increases in global warming GCM experiments. J Clim 21:6141–6155

Stevens B, Brogniez H, Kiemle C, Lacour J-L, Crevoisier C, Kiliani J (2017) Structure and dynamical influence of water vapor in the lower tropical troposphere. Surv Geophys. doi:10.1007/s10712-017-9420-8

Takemi T, Satomura T (2000) Numerical experiments on the mechanisms for the development and maintenance of long-lived squall lines in dry environments. J Atmos Sci 57:1718–1740

Tulich S, Mapes BE (2010) Transient environmental sensitivities of explicitly simulated tropical convection. J Atmos Sci 67:923–940. doi:10.1175/2009JAS3277.1

Vial J, Dufresne J-L, Bony S (2013) On the interpretation of inter-model spread in CMIP5 climate sensitivity estimates. Clim Dyn 41:3339–3362

Wing AA, Emanuel K, Holloway CE, Muller C (2017) Convective self-aggregation in numerical simulations: a review. Surv Geophys. doi:10.1007/s10712-017-9408-4

Zhang J, Zuidema P, Turner D, Cadeddu M (2017) Tropical humidity vertical structure inferred from a microwave radiometer over the equatorial Indian Ocean. J Appl Meteorol